



REEL Demo – Romande Energie ELectric network in local balance Demonstrator

Deliverable: 3d4 Models for the optimization of grid
penetration of smart DSM in different grid topologies

Demo site: Rolle

Developed by

Vasco Medici, ISAAC, SUPSI

Federico Rosato, ISAAC, SUPSI

Davide Strepparava, ISAAC, SUPSI

Lorenzo Nespoli, ISAAC, SUPSI

Roman Rudel, ISAAC, SUPSI

[Canobbio, 25.03.2021]

1 Description of deliverable and goal

Careful planning for the use of technologies such as smart meters, storage, and demand-side management systems has enormous potential to facilitate the transition to an energy system less dependent on non-renewable sources. A new system of active management of the electricity distribution grid will allow to minimize the costs generated by the introduction of photovoltaic production, electrification of heating systems and the advent of electric mobility, which are technologies that stress the distribution grid, and that, if not well managed, can generate significant costs for distribution system operators (DSOs).

The purpose of this work is to develop a tool to evaluate the potential of demand side management (DSM) in counteracting these adverse effects in simulation, on realistic grid topologies.

1.1 Executive summary

In this deliverable, we present a methodology that, given a certain region, allows to design a plausible distribution network and to populate it with plausible loads. On this synthetic network it is then possible to test different penetration scenarios of photovoltaic (PV) generation, electric heating via heat pumps, and electric mobility. All this is integrated in a simulation environment that allows performing a power-flow study on the synthetic grid and testing the effect of DSM control algorithms for grid optimization. The DSM tested algorithms are based on model predictive control (MPC) techniques and rely on realistic predictions of load and production curves on the network and could therefore be used in the real world. In this deliverable, we present a particular example of such a methodology applied to the study of the effect of vehicle to grid (V2G) for energy management.

1.2 Research question

The research question that the methodology presented in this deliverable attempts to answer is the following. Is it possible to evaluate quantitatively and with sufficient accuracy the impact of DSM algorithms in a given configuration of:

- network topology
- loads configuration (residential, commercial, industrial, ...)
- penetration of PV generation
- penetration of heat pumps for space heating the domestic hot water
- penetration of electric vehicles (EVs)
- penetration of smart DSM algorithms

1.3 Novelty of the proposed solutions compared to the state-of-art

The proposed methodology allows testing the effectiveness of specific DSM solutions (possibly combined with local storage) under various scenarios. Such a procedure can be used to evaluate the effectiveness of smart DSM (with different control algorithms) from a techno-economic point of view in multiple situations. A natural continuation of this work is the identification of network archetypes through clustering. The clustering should be performed so that one could associate the most promising DSM strategy and its effectiveness to each network archetype. A specific combination of such archetypes should be able to represent DSO grids generally and could be used to identify what technologies to adopt and where to concentrate them to optimize costs of the grid infrastructure.

1.4 Description

The simulation environment includes all the components that are needed to perform both technical and economic analysis, following the concept depicted in figure 1. The

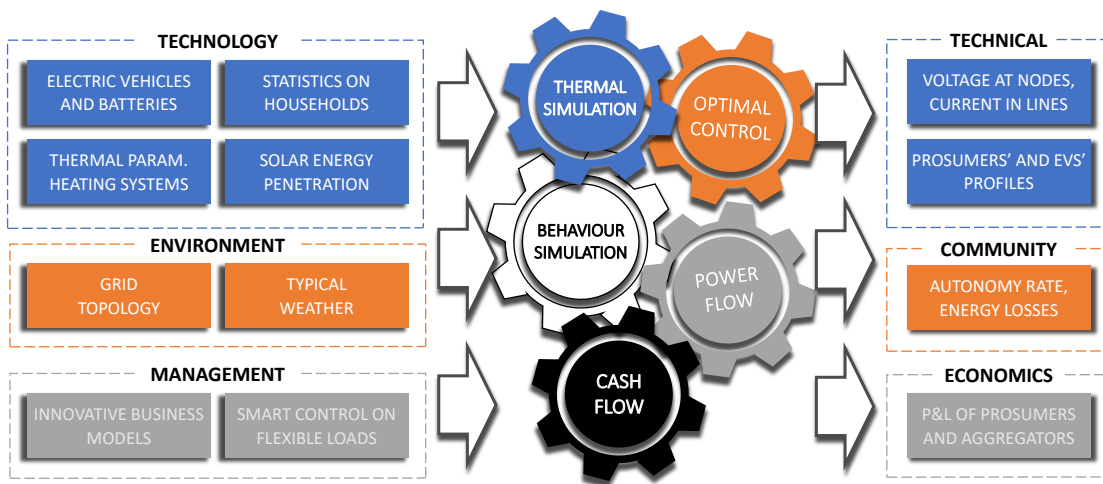


Figure 1: Simulation concept

simulation software provides the possibility to simulate algorithmic agents interacting with the grid. A scheme for the simulator is provided in Figure 2. The agents can be simulated in parallel, since communication based on message-exchanging through a central message broker. The main driving script executes the simulation and, at each step, launches the parallel agent simulation with a message containing information about the newly simulated electrical step (such as the voltage at the agent node, etc.), if needed to decide the next course of action. Individual agents can include an arbitrary number of individual physical components such as building thermal envelopes, heating terminals, boilers, heat pumps, batteries, electric vehicles, etc. Each of these elements has a corresponding physical model code, configured with parameters specific to the agents' instance. Both the model and the agents can send, through the central message broker, records of their internal state

to a time-series database (InfluxDB), allowing for storage and subsequent analysis of the simulation results. Both the electrical quantities and the agents' internal evolving state are, therefore, recorded. Furthermore, the same time-series database stores useful information available to the agents, such as meteorological data, temperature and irradiance.

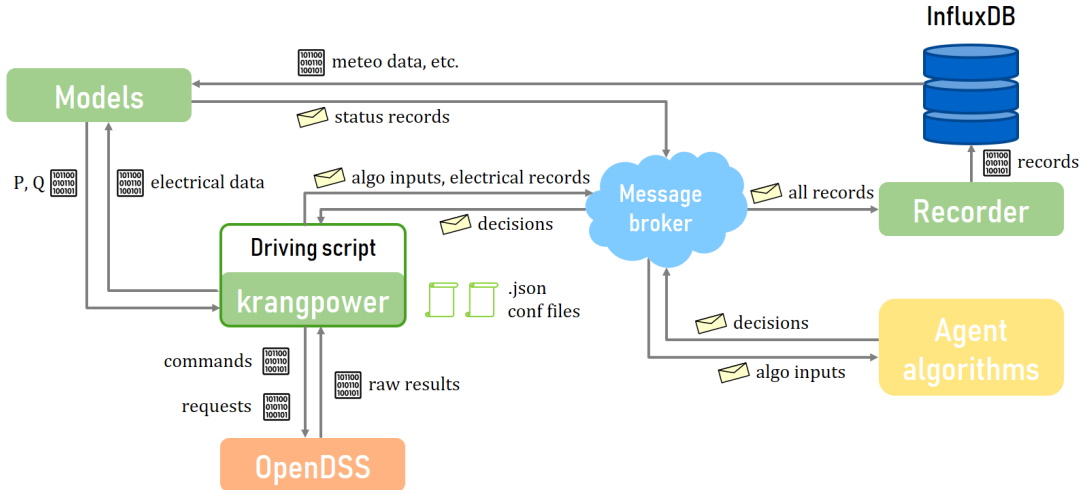


Figure 2: Conceptual scheme of the simulator

In the next subsections, we will describe the most important components of the simulation and finally we will present a case study in which the effect of bi-directional charge control of EVs will be applied to the case of a grid with extreme PV and EV penetration.

1.4.1 Grid topology design

A tool for generating realistic distribution grids was developed. Relative to current existing solutions [1, 2, 3], the aims of the tool were to allow inter-building connections, consideration of geographical obstacles and promote a clustering of the loads aware of the available substation sizes, thus capable of fitting the size to the cluster to one size in a reasonably efficient way. The tool is able to generate a grid for an existing community, drawing data from a publicly available source (specifically, the current implementation uses OpenStreetMaps as a source for geographical data). The data extracted comprise building position and area and the street paths. The nominal power of the building is estimated starting from its area.

Initially, the streets form a connected graph induced by the street segments, while the buildings are isolated points. The next step, then, is the creation of an underlying, highly connected graph comprising all the possible connections to be considered. The buildings are connected to the street segments defined by the four nearest street points; the shortest path is drawn, so the connection to the segment is either orthogonal or at one of the ends. Furthermore, the buildings are connected to their 2 nearest peers, ensuring that "daisy-chain"-style connections are considered and selected, if economical. A cost is then assigned to each edge. In the current ver-

sion, a base cost is evaluated only according to the length of the connection and its type (street-street, building-street, building-building). This part was conceived while keeping in mind an easy and important extension, that can be straightforwardly integrated: additional information about the underlying terrain and, possibly, obstacles, can be factored in the costs, in order to evaluate more accurately the feasibility of connections.

Once the base graph is in place, we can generate a first version of the clustering. We focused on tree clustering techniques for application to the minimum spanning tree of the underlying graph. Algorithms such as TAHC [4], while returning clusters of high quality, have an inherent problem that makes them unsuitable for the task at hand: they do not have any way of governing the maximum size of the clusters. Often, this leads to severely unbalanced clusters that are impossible to reduce to existing substation sizes. The final choice fell on a classic tree clustering algorithm, LUKES [5]. This algorithm presents several advantages: it directly supports a maximum size of the cluster in terms of node weights (that map, in our application, to customer powers), it yields the optimal solution in terms of cut edges cost and it runs in pseudo-polynomial time (parametrized by the maximum size selected). Nevertheless, the bare application of this algorithm, in general, brings to cluster sizes that may be very small or just above one of the available substation sizes, thus resulting in an inefficient allocation. We devised a method for finding a reallocation of the loads among the clusters in a way that better fits the available sizes. We proceed in the following way. With reference to a single one of the clusters, we first identify a suitable boundary with an alpha-shape (a generalization of the concept of convex hull allowing for radius-limited concavity). We consider as boundary nodes the ones that are directly touched by this boundary line and have neighbors in one or more other clusters. For each one of this nodes, we find cuts of the underlying cluster MST such that the part containing the boundary node is under a certain, configurable size in terms of node weights; these are considered as candidate for reallocations to one of the cluster neighboring the reference boundary node. Once we have considered all such possible reallocations, we make the following consideration. Two reallocations are compatible if the nodes transferred by the first do not include a node the second wants to use as attachment point. This relationship between two reallocations induces a Compatibility Graph, in which the nodes are the reallocations and an edge exists if two reallocations are compatible in this sense. Cliques (complete subgraphs) in the compatibility graph are groups of moves that can be all executed together; see figure 3.

Taking into account all the possible reallocations, nevertheless, would be too computationally heavy. But there is a certain amount of redundancy in the relocation, in the sense that two reallocation of close size between the same two ordered clusters will have very similar effect on the final solution, so we need not consider them all. We can arrange the reallocations for each cluster pair in bins (the width of the bins is taken to be the minimum reallocation size), and we retain only one reallocation

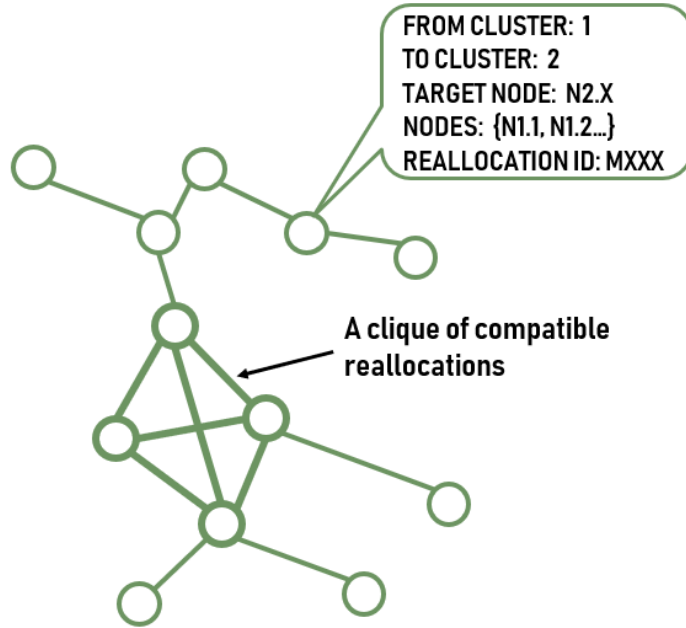


Figure 3: Visual representation of the compatibility graph, with a clique of compatible reallocations

per bin; this typically causes a dramatic reduction in the number of reallocations. See figure 4 for a representation of the bins of similar reallocations.

We then proceed to enumerate all the cliques and we evaluate them in terms of global substations+connections cost. At this point we can take another important shortcut. To have a chance at profitability, a clique of reallocations must involve at least one reallocation that allows the reduction of a substation; otherwise, being Lukes clustering optimal, the cost would surely increase. Thus, cliques that do not meet this criterion are immediately discarded before evaluation. The clique that grants the best cost improvement is then retained and the reallocations are applied to get the final solution. Once the clusters are in place, we refine the connections by considering the underlying connected graph once more and calculating a Steiner tree approximation that touches all the loads for each cluster. We are now ready for grid sizing. The current version of the method places the substation on the edge that exhibits maximum edge betweenness centrality, and then for each edge a diversified load is calculated (equal to the sum of the loads hierarchically below that edge, taking the substation as the root, multiplied by a diversity factor). A unique coefficient for each cluster is then evaluated for transition from the diversified load to line impedance, and this coefficient is selected in order to obtain a maximum, configurable delta V.

1.4.2 Electrical simulation

The electrical power flow simulation is carried out with Krangpower, an internally developed Python library able to interact with OpenDSS, which we released open-

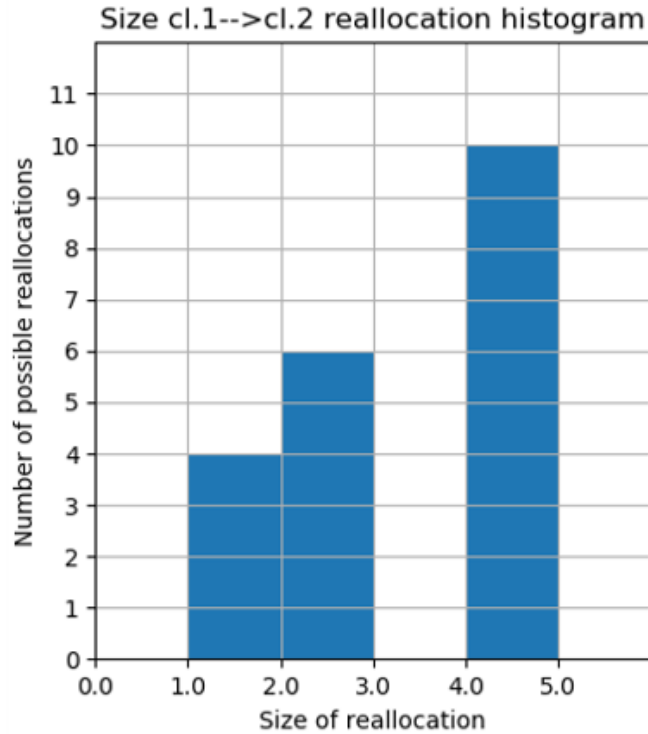


Figure 4: Bins of reallocations of similar sizes

source¹. It allows accessing the different functionalities of OpenDSS within the simulation framework by providing modern interfaces, such as structured information retrieval, dynamic querying, graphing, and other such functionality, in order to provide a systematized interface and avoid the continuous need for scripts custom-tailored to the particular simulation.

The configuration of the simulation can get quite complicated, since full information must be provided about the grid, the agents, the models they contain with all the possible parameters. The file type used is JSON, due to the inherent hierarchical structure, useful for specifying the agents, then their content, and then their parameter. Krangpower uses a specifically structured JSON file that contains information about the grid, essentially a list of elements (for example, transformers and lines) with their parameters and topological information about the buses they are connected to.

1.4.3 Weather conditions

For the specific scenarios studied, a typical meteorological year (TMY) is simulated. The meteorological dataset is essential to have correct and synchronized user behaviors and to simulate solar power generation with a reasonable statistical distribution over the year. The TMY is generated using the commercial tool Meteonorm², the world's leading provider of synthetic datasets for meteorological assessments for re-

¹<https://github.com/supsi-dacd-isaac/krangpower>

²www.meteonorm.com

newable power plants and other engineering purposes.

1.4.4 Consumption profiles of residential and commercial users

Each building in the map is automatically connected to the synthetic grid and a consumption profile is associated to it. The building's intended use and thermal characteristics are picked from regional statistics, or where available from real data. To simulate residential users' energy consumption profiles, we used Load Profile Generator³ (LPG), a tool also available as an open-source library⁴. LPG is an agent-based simulation tool that performs a full behaviour simulation of the people in a household and uses it to generate load curves, water consumption profiles and car usage profiles. All three types of profiles are used in our simulation environment. Thousands of different profiles have been simulated with LPG. Every user has a specific synthetic energy profile, and their aggregation has a realistic simultaneity factor. All the profiles of the appliances come from real measurements and are properly considering active and reactive power. We randomly assign the small loads to one of the 3 phases, while the loads requiring more than 10A are equally split and assigned to 2 or 3 phases. Thanks to the users' LPG profiles, it is also possible to define when users are at home or are travelling. In this way, the profiles of the appliances and the EV plug state are coherently synchronised.

For the commercial users, we used a library developed by Hive Power⁵ to simulate different type of businesses, which is compliant with the SIA norm 2024 / 2015 [6]. These profiles generated using this library are also following some stochastic behaviour to represent in a correct way simultaneous loads from different offices and make use of the global horizontal irradiance from the weather profile to simulate the need for lighting.

Consumption profiles due to heating and cooling are modeled separately and only the water consumption profiles from LPG are fed to the models that are generating them. A detail explanation of the thermal simulation is available in section 1.4.5.

1.4.5 Thermal loads

In order to obtain a representative dataset for Switzerland, we used the STASCH standard [7] and its variants as a reference for the heating system and the control logic. In particular we implemented STASCH6, which includes both space heating and domestic hot water production. The STASCH6 standard comprehends 3 main components: a heatpump (HP), a water tank used as an energy buffer, and a heating element delivering heat to the building. The control logic is explained in detail in annex A.1.

³www.loadprofilegenerator.de

⁴<https://github.com/FZJ-IEK3-VSA/LoadProfileGenerator>

⁵www.hivepower.tech

Building model We modeled the building thermal dynamics with a simple one state RC equivalent model, as done in [8]. The main reason for this choice is that it is hard to generalize RC models with higher number of states, since no values can be found in the literature for the needed parameters. Estimating an RC model from data requires different measurements of temperatures, internal and solar gains, at a resolution of at least 10 minutes. This kind of datasets are extremely hard to find, and limited to only a few, often undwelled, cases. These equivalent RC circuit parameters could, in theory, be estimated starting from first principles, however recently proposed studies show that this can give worse results than estimating a model from data [9]. The second reason is that, while a higher order model leads in general to smaller one step ahead residuals compared to a lower order model, the loss of accuracy passing from a one state model to an higher order one when considering a longer period of simulation is much lower [10]. Last, when considering RC models for buildings with a number of states higher than 3, the chances of overfitting are high, and additional measurements such as the heat fluxes between thermal zones are required to guarantee observability. Alternatively, pseudo-random binary sequences can be applied to the heating systems in order to excite the system in a wide range of frequencies [11], while being uncorrelated with other exogenous inputs. This technique induces high changes in internal temperature of the building and cannot clearly be applied to occupied buildings.

The final model is the following;

$$C \frac{\partial T_z}{\partial t} = \frac{T_{ext} - T_z}{R} + kQ_h + A_{eq}I_s \quad (1)$$

where T_{ext} is the the external temperature, R is the equivalent thermal resistance for the building, C is the thermal capacitance, k is a parameter weighting the estimated power coming from the heating system Q_h , I_s is the incoming solar radiation and A_{eq} is the estimated equivalent window area. In order to obtain representative simulations, R , C , k and A_{eq} were estimated from statistical data for Swiss households. For the simulation regarding the LIC pilot, R was directly estimated from data and C and A_{eq} were estimated from the buildings' equivalent area.

At Swiss level, in a future version the thermal characteristics of the building will be linked with the map of the demand from residential and commercial buildings provided by the Swiss Federal Office of Energy in the GEO Admin API⁶, which are based on the Federal Statistical Office's 2014 Buildings and Dwellings Statistics and 2013 Statistics on Company Structures, and the Federal Office of Energy's figures in the annual report 'Energy consumption in the industry and services sector'.

Floor heating The heat distribution system that allows to transfer the required heat from the storage tanks to the building was designed from first principles. A heating system based on serpentine was modeled, the details are presented in An-

⁶https://map.geo.admin.ch/?layers=ch.bfe.fernwaerme-nachfrage_wohn_dienstleistungsgebäude&lang=en

nex A.2.

Water tanks The water tanks connected with the floor heating, which are used as a buffer by the heat pump, and those used for domestic hot water (DHW) are modeled as N-states fully-mixed stratified tanks. Despite not being able to model buoyancy driven effects such as heat plumes and transient de-stratification, this kind of models are suitable for 1D simulations and control [12]. A detailed description of the model can be found in Annex A.3.

Heat pump model The heat pump is modeled by means of interpolated tables, in which heating and electrical power are available as a function of the evaporator and the condenser temperatures. The tables were taken from the energy simulation software Polysun⁷. When the heat pump produces heat for both the heating system and the domestic hot water, its control logic prioritizes the latter, meaning that the buffer is heated as long as the DHW tank temperature sensor reaches the upper bound of its hysteresis control.

1.4.6 PV model

Residential PV power plants were modeled using the Sandia National Laboratories PV Collaborative Toolbox [13], which is based on the 1985 Grover Hughes' Engineering Astronomy course at Sandia National Laboratories. The global horizontal irradiance from the weather model is projected into the plane of the PV array and the AC power produced by it is calculated assuming standard poly-crystalline modules are used.

1.4.7 EV and stationary battery models

Both stationary batteries and EVs have been modelled as a one state dynamic system with asymmetric charging and discharging efficiencies, self-discharge, and a minimum charging and discharging power. The detailed description of the EV dynamics is available in annex B.1.

Unlike stationary batteries, EVs also have a usage profile related to their primary function, which is to provide a mobility service. Following the users' behaviours defined by the LPG, it has been possible to also define the usage of EVs, including the purpose of the trips and the consequent mileage and timing of departure/arrival. The yearly mileage of EVs has been defined to follow a distribution centered around the average Swiss total annual mobility per person with private motorized traffic, made available by the EVA ERA-Net project⁸.

⁷www.velasolaris.com

⁸<https://evaproject.eu/>

1. **A baseline scenario.** In this scenario, the EVs are charged at the charging station's nominal power as soon as they are plugged to it.
2. **Smart DSM scenario.** In this scenario, EVs coordinate with each other to achieve the objective function of reducing fluctuations at the transformer. Charging power can range from a minimum of 1.38kW (single-phase 6A) to a maximum represented by the charger's rated power, in this case 11kW (three-phase 16A). The optimization problem ensures that the cars are fully charged when the user picks them up.

V2G control strategy The distributed control approach applied in the smart DSM scenario assumes a virtual energy community setting. It is described in detail in Annex B.2, while its mathematical foundation and its applicability to a multi-level distributed optimization setting are discussed in [14] and [15], respectively. The distributed control has the capability to maximize the welfare of a community that is subject to dynamic prices and explicit grid constraints while ensuring to reach a generalized Nash equilibrium. We use it here in a simplified way to minimize power fluctuations at the transformer by reducing the global objective function to the sum of the transformer's squared power over a 24h horizon. Technically, to achieve this, α_i (Eq. 42) was set to 1 for all agents, a power tariff was applied to the transformer (which in this case represents the coupling point of the virtual community) by introducing the γ coefficient (Eq. 47) and the energy prices were set to 0. This ensures that all agents are contributing to the best of their ability to the overall objective function without worrying about their own costs. Of course, this is an extreme scenario. In this case, the one who will demand this flexibility service to its users on the network will have to cover the additional user costs caused by the activation of the EV battery. But it shows the potential technical boundaries of DSM actions, regardless of financial requirements.

Simulation results Since the coordination mechanism is an iterative procedure that can be time-consuming, we did not simulate an entire year. Instead, we simulated the day with the maximum power consumption (a day in January of our simulated TMY) and the day with the maximum power injection into the grid (a day in June). Indeed, the introduction of PV and EV into the grid increases power excursions to the transformer in both directions, and so it is important to check both boundary cases. In winter, the power required by EVs is added to that already required by heaters and, in general, by loads that cannot be controlled and contributes to increasing the evening peak. In summer, the PV obviously injects a lot of energy around noon and causes the power flow to reverse.

Ideally, a DSM algorithm would need to limit such power excursions, in both directions. First of all, to avoid exceeding the transformer's operational limits and secondly, to reduce its ageing, as distribution transformers were not originally designed to accommodate such big power excursions and reverse power flows [16].

To qualitatively assess the effect of DSM on the transformer’s power, we plotted its time course along with the total controlled power (i.e. the total power of the EVs) for the two simulated days. The results as shown in Figure 6. It is meaningful to note

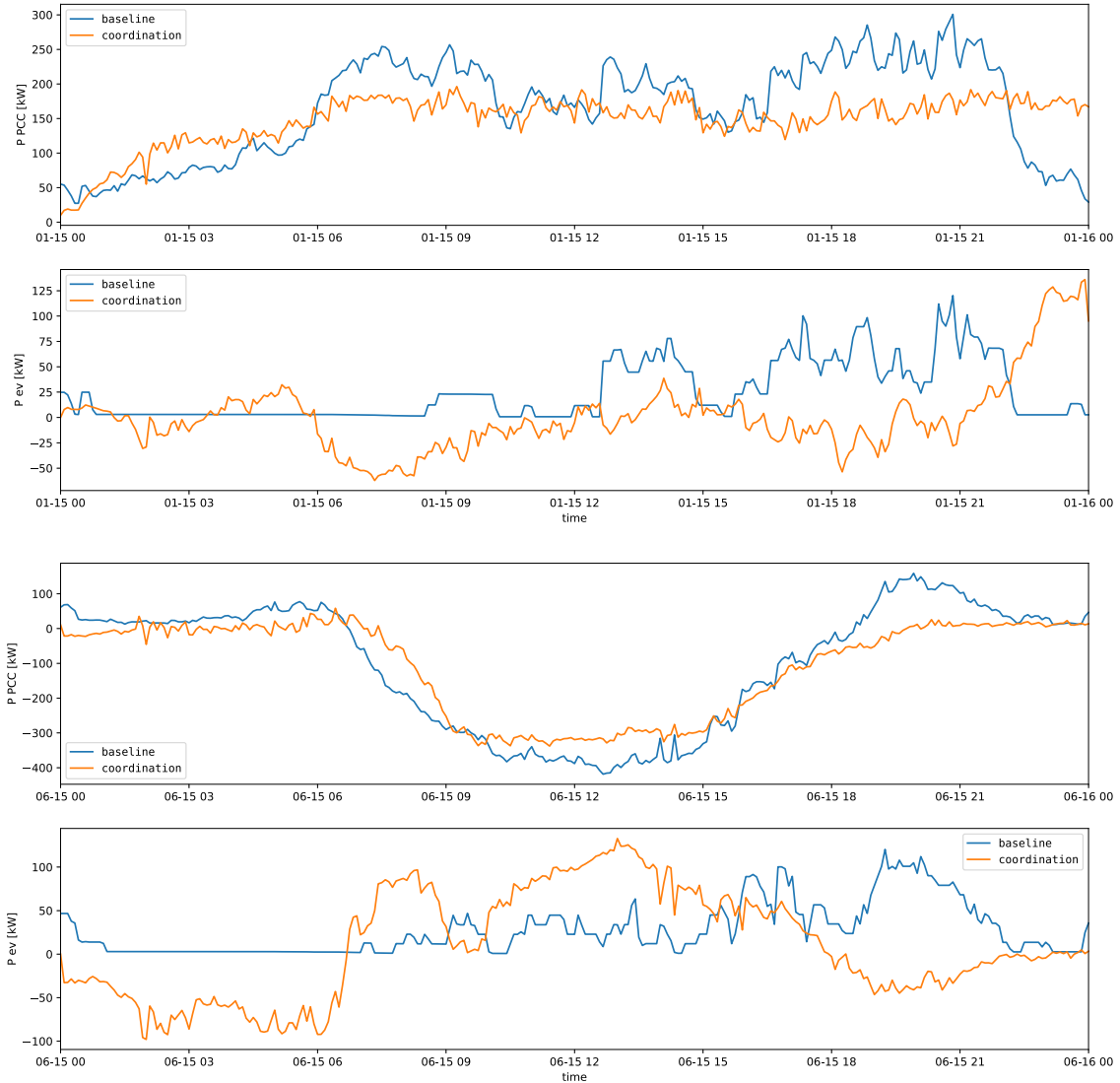


Figure 6: Active power at the transformer and total power of the EVs. Top: day with the maximum power consumption at the transformer. Bottom: day with the maximum power injection at the transformer.

that in both cases the EVs are able to reduce the power excursions at the transformer. In this case, it is important to emphasize that the control algorithms are based on a realistic forecast. This is not the ideal solution with perfect forecast, but a realistic one, which depends on the quality of the forecast. An in-depth discussion of this issue is available in [17]. Furthermore, the control loop currently runs with a time granularity of 5 minutes. It would be conceivable to increase this frequency. However, at the moment it is not realistic to imagine a real-time DSM system based on EV, as the loaders are not able to do it.

This means that the risk of exceeding the operating limits of the transformer is not

fully mitigated. Nevertheless, it is conceivable to add a battery in the network, which has the possibility to be operated in real-time. And the combination of the current DSM strategy with real-time control of a battery has the advantage of reducing its required capacity.

Figure 7 focuses on the voltage at the PQ buses. The voltage between line and neutral is plotted for all terminal nodes in the network and for all phases (this is in fact an unbalanced load flow simulation).

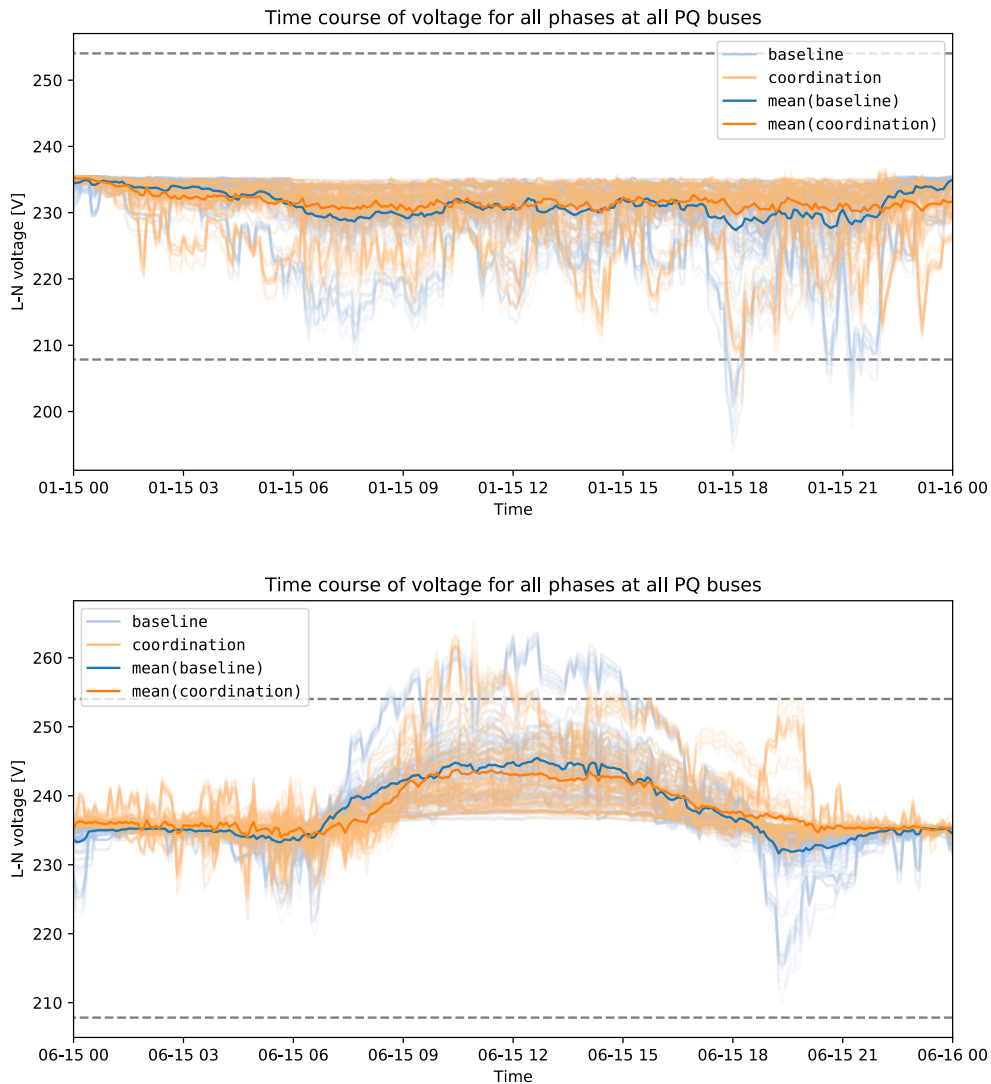


Figure 7: L-N voltage at all nodes and all phases in the PQ buses of the grid. Top: day with the maximum power consumption at the transformer. Bottom: day with the maximum power injection at the transformer. Grey dashed lines: $\pm 10\%$ limits from nominal voltage $400/\sqrt{3}$.

It can be seen that the voltage is a more local phenomenon that requires targeted interventions. Although the DSM algorithms partially succeed in mitigating voltage problems at the nodes, some nodes still violate the EN50160 standard [18], espe-

cially in the day with the highest PV injection. The algorithm used here does not account for voltage and merely optimizes the total power at the transformer. Specific network constraints on voltage could be enforced using Lagrangian multipliers (see Annex B.2). In this case, one would use the voltage sensitivity coefficients as a first approximation of EV power's effect on the voltage. However, EVs' presence is not always guaranteed, and at such a local level, it would be hard to assure that the voltage quality standards are respected at all times. In this case, it would be advisable for the DSO to reinforce the weakest lines or to rewire its grid. Alternatively, the DSO could use our simulation tool to select where to site the above mentioned stationary battery so that both "local" voltage and "global" power constraints are respected.

1.5 Regulatory and legal barriers for implementation

In this deliverable, we presented a generic simulation tool that allows performing a techno-economic evaluation of DSM strategies. This tool can be used to evaluate the effect of business models and market designs, which, in order to be implemented, would require a modification of the current legislation. Consequently, it has the potential to allow overcoming possible barriers by providing quantitative data in support of the need for a change.

2 Achievement of deliverable

2.1 Date

March 2021.

2.2 Demonstration of the deliverable

The demonstration is provided using a case study, presented in section 1.4.8.

3 Impact

The work presented in this deliverable demonstrates the potential of the simulation tool developed by ISAAC-SUPSI in the REeL project. The tool allows to couple a detailed simulation, of consumption (including thermal loads) and production (in this case, PV), with control algorithms of different types (including distributed ones). The control algorithms are based on a realistic forecasting system that uses state of the art methods. This tool can be used to reduce the impact of distributed renewables on the grid and to test alternative business models involving the control of distributed flexibility in the local grid.

A Annex: Heating system models

A.1 Control logic of heating systems

The heat pump control logic is based on two temperature sensors placed at different heights of the water tank, while the circulation pump connecting the tank with the building's heating element is controlled by an hysteresis on the temperature measure by a sensor placed inside the house.

We describe the control logic in a sequential way, following the heating components of the system. The first decision is taken by the building central controller, which decides its working mode, that is, if the building needs to be cooled or heated, based on a moving average of the historical data of the external temperature:

$$\begin{cases} wm_t = -1 & \mathbf{if} \ T_{ma,t} > T_{max,ma} \\ wm_t = 1 & \mathbf{if} \ T_{ma,t} < T_{min,ma} \\ wm_t = 0 & \textit{otherwise} \end{cases} \quad (2)$$

where the working mode wm_t is negative when the building requires to be cooled, positive when heating is required, and 0 when no actions are needed. $T_{max,ma}$ and $T_{min,ma}$ represent the maximum and minimum values of the external temperature's moving average, which is based on the past 7 days. The actual activation of the heating element is controlled by the hysteresis on the internal temperature of the building, T_z . If the working mode is positive, this is given by:

$$\begin{cases} s_{hy,t} = 1 & \mathbf{if} \ (T_z < T_{min,hy} - \Delta T/2) \\ & \mathbf{or} \ (T_z < T_{min,hy} + \Delta T/2 \ \mathbf{and} \ s_{hy,t-1}) \\ s_{hy} = 0 & \textit{otherwise} \end{cases} \quad (3)$$

where $s_{hy,t}$ is the state of the hysteresis at time t , 1 meaning that the circulation pump of the heating element must be activated, and ΔT was chosen to be equal to $1^\circ C$. For completeness, we report also the control logic when the building is in cooling mode:

$$\begin{cases} s_{hy,t} = 1 & \mathbf{if} \ (T_z > T_{max,hy} + \Delta T/2) \\ & \mathbf{or} \ (T_z > T_{max,hy} - \Delta T/2 \ \mathbf{and} \ s_{hy,t-1}) \\ s_{hy} = 0 & \textit{otherwise} \end{cases} \quad (4)$$

The incoming water temperature in the heating element is then modulated linearly through a 3-way valve between a maximum and minimum value, based on the external temperature, both in the heating and cooling modes. When operative, the

heating element requests hot or cold water to the water tank, which control logic is based on two temperature sensors located in two different layers. When the building is in heating mode, the control logic is a simple hysteresis based on the temperature of the sensor in the uppermost layer, which is identical to the one in (3). When in cooling mode, the control logic is the following:

$$\begin{cases} s_{hy,t} = -1 & \mathbf{if} \ (T_{up} > T_{max}^c + \Delta T/2) \\ & \mathbf{or} \ T_{low} > T_{max}^c + \Delta T/2 \\ s_{hy,t} = 0 & \mathbf{if} \ (T_{low} < T_{min}^c) \ \mathbf{or} \ (T_{up} < T_{max}^c - \Delta T/2) \\ s_{hy,t} = s_{hy,t-1} & \mathit{otherwise} \end{cases} \quad (5)$$

where T_{up} and T_{low} are the temperature measured by the upper and lower sensors, respectively, and T_{min}^c and T_{max}^c are the minimum and maximum desired temperatures of the water in the tank while in cooling mode.

The value of $s_{hy,t}$ is then communicated to the HP. In the case in which the HP is also used for the domestic hot water (DHW), the DHW tank is always served with priority by the HP.

A.2 Heat distribution system

Floor heating was modeled starting from first principles. Considering a fixed and uniform temperature for the ground and the building internal temperature at each time-step and stationary conditions, we can retrieve the analytical expression of the temperature profile along the pipe, through the energy balance on an infinitesimal element of the pipe. This can be expressed as:

$$\frac{\partial cT_x}{\partial t} = \Phi_x - \Phi_{x+\partial x} + \dot{q}_{up} + \dot{q}_{down} \quad (6)$$

where c is the heat capacity in J/K , x is the distance from the pipe entrance, T_x is the temperature of the water inside the pipe at x , Φ are enthalpy flows at the entrance and exit of the considered infinitesimal volume, \dot{q}_{up} and \dot{q}_{down} are the heating powers from the building and from the ground. Expressing the latter through equivalent resistance taking into account convective and conductive effects, the balance in steady state can be rewritten as:

$$\frac{\dot{m}c_p}{\rho^*} \frac{\partial T_x}{\partial x} = \frac{R_{down}T_z + R_{up}T_g}{R_{down} + R_{up}} - T_x = T^a - T_x \quad (7)$$

where T^a is the asymptotic temperature and where:

$$R_{down} = \frac{1}{h_{in}w} + \frac{1}{h_{u,eq}w} + R_u \quad (8)$$

$$R_{up} = \frac{1}{h_{in}w} + R_g \quad (9)$$

$$\rho^* = \frac{R_{up} + R_{down}}{R_{up}R_{down}} \quad (10)$$

where w is the diameter of the tube, h_{in} is the internal coefficient of heat transfer, which can be retrieved using available empirical relation for fully developed flow with fixed temperature at the boundary conditions [19], $h_{u,eq}$ is the heat transfer coefficient between the floor and the building air including both the effect for natural convection and radiation. The values of $h_{u,eq}$ can be found in the literature [20],[21]. The value of the thermal resistances R_u and R_g , towards the floor and the ground, can be found in the literature as well. We can reformulate (7), making it adimensional through a change of variable:

$$\frac{\partial \Theta}{\partial \mathcal{X}} = -\Theta \quad (11)$$

from which solution we can retrieve the temperature profile of the water inside the pipe:

$$T_x = T^a + (T_0 - T^a)e^{\frac{-x\rho^*}{\dot{m}c_p}} \quad (12)$$

where T_0 is the temperature of the water at the pipe inlet. We can use (12) to retrieve the heating power flowing into the building, integrating $\dot{q}_{up}(x)$ along the pipe.

$$\dot{Q}_{up} = \int_0^L \dot{q}_{up}(x)dx = \int_0^L \frac{T(x) - T_z}{R_{up}} dx \quad (13)$$

where L is the length of the serpentine. Integrating, we obtain

$$\dot{Q}_{up} = \frac{(T^a - T_z)L - (T_L - T_0)\frac{\dot{m}c_p}{\rho^*}}{R_{up}} \quad (14)$$

where T_L is the temperature of the water at the outlet of the serpentine. Note that the equation (14) tends to $(T_L - T_0)\dot{m}c_p$ when R_{down} increase and R_{up} is kept fixed. The nominal mass flow of the heating system and the length of the serpentine are found as the solution of the following optimization problem:

$$\operatorname{argmin}_{L, \dot{m}} \left(\dot{Q}_{up}(L) - \dot{Q}_{nom} \right)^2 + 10^{-3} (\dot{m} - \dot{m}_{nom})^2 \quad (15)$$

where \dot{m}_{nom} is a reference mass flow, equal to $0.1 [kg/s]$ and \dot{Q}_{nom} is the power required to keep the building internal temperature constant under reference conditions (we used an external temperature of $-4^\circ C$ and a desired internal temperature

of 20 °C):

$$\dot{Q}_{nom} = \frac{\Delta T_{ref}}{R} \quad (16)$$

where R is the resistance of an equivalent RC circuit describing the heating dynamics of the building.

A.3 Water tank model

The dynamic equation describing the evolution of the temperature of the tank's layers is the following:

$$C \frac{\partial T_i}{\partial t} = \dot{Q}_{buo,i}^u + \dot{Q}_{buo,i}^d + \dot{Q}_{h,i} + \dot{Q}_{loss,i} + \dot{Q}_{cond,i}^u + \dot{Q}_{cond,i}^d + c_p \dot{m}(T_{i-1} - T_i) \quad (17)$$

where T_i is the temperature of the i_{th} layer, $Q_{buo}^u, Q_{buo}^d, Q_{cond}^u, Q_{cond}^d$ are the thermal powers due to buoyancy and conduction, from the lower and upper layer, respectively. The last term represents the enthalpy flow due to mass exchange, while C is the thermal capacity of the layer, in $[J/K]$ and $Q_{h,i}$ is the thermal power due to an electric resistance (for the boiler) or an heat exchange (for the heating system buffer). The expression for the above thermal power are the following:

$$\dot{Q}_{buo,i}^u = k \max(T_{i+1} - T_i, 0)N, \quad 0 \quad \text{for } i = N \quad (18)$$

$$\dot{Q}_{buo,i}^d = k \max(T_{i-1} - T_i, 0)N, \quad 0 \quad \text{for } i = 1 \quad (19)$$

$$\dot{Q}_{cond,i}^u = u_{amb}(T_{i+1} - T_i), \quad 0 \quad \text{for } i = N \quad (20)$$

$$\dot{Q}_{cond,i}^d = u_{amb}(T_{i-1} - T_i), \quad 0 \quad \text{for } i = 1 \quad (21)$$

$$\dot{Q}_{loss,i} = u_{amb}(T_{ext} - T_i) \quad (22)$$

$$\dot{Q}_{h,i} = \dot{Q}_{tot}/n_h \quad \text{if } i \in \mathcal{I} \quad (23)$$

$$(24)$$

where N is the number of layers, u_{amb} is the equivalent thermal loss coefficient with the ambient and \mathcal{I} is the set of the n_h layers heated by the heat exchange (or electric resistance). The buoyancy model is the one proposed in the IDEAS library [22]. Detailed description of the parameters for the boiler model can be found in [23].

B Annex: Optimization of EV charging and discharging

B.1 Detailed EV model description

The EV's charging strategies we designed require the solution of an optimization problem, which is formulated as a mixed integer quadratic problem (MIQP), in which a (usually) economic objective is minimized. In the following, we present the core EV optimization problem. Different charging strategies differ in the specification of the objective function, while the set of constraints remains unchanged.

Called $u = [p_{ch}^T, p_{ds}^T]^T \in \mathbb{R}^{2T}$ the vector of concatenated decision variables for the

control horizon T , where p_{ch} and p_{ds} are the battery charging and discharging power, respectively, $\tilde{u} = [p_{ch}, p_{ds}] \in \mathbb{R}^{T \times 2}$ being the same vector reshaped in a 2 columns matrix, $\hat{p} \in \mathbb{R}^T$ being the forecasted power at building's main for the next control horizon, $y \in \mathbb{R}^T$ being an auxiliary variable representing the energy costs at each time step, we seek to solve the following problem:

$$u^*, y^* = \underset{u, y}{\operatorname{argmin}} \sum_t^T y_t + k_1 \|\delta_x\|_2^2 + k_2 \|\delta_e\|_1 \quad (25)$$

$$x_{t+1} = Ax_t + B\tilde{u}^T \quad \forall t \in [2 \dots T] \quad (26)$$

$$x_{min} - \delta_x \preceq x \preceq x_{max} \quad (27)$$

$$x \succcurlyeq e_{min} + \delta_e \quad (28)$$

$$\delta_x \geq 0 \quad \delta_e \geq 0 \quad (29)$$

$$0 \preceq a \preceq x_{plug} \quad (30)$$

$$a[1, 1]^T \leq 1 \quad (31)$$

$$a \circ \tilde{u}_{min} \preceq \tilde{u} \preceq a \circ \tilde{u}_{max} \quad (32)$$

$$y \succcurlyeq p_{buy} (\tilde{u}[1, -1]^T + \hat{p}) \quad (33)$$

$$y \succcurlyeq p_{sell} (\tilde{u}[1, -1]^T + \hat{p}) \quad (34)$$

$$(35)$$

where \succcurlyeq stands for $\succcurlyeq_{\mathbb{R}_+}$, indicating element-wise inequalities, and \circ represents the Hadamard product (element-wise multiplication). For sake of clarity, we start explaining the problem constraints and the variables involved, and we finally explain the objective function (25) at the end of the exposition.

Equation (26) describes the EV battery's dynamics. $A \in \mathbb{R}_+$ and $B \in \mathbb{R}_+^{1 \times 2}$ are the discrete dynamics matrices obtained by the continuous one through exact discretization [24]:

$$\begin{aligned} A &= e^{A_c dt} \\ B &= A_c^{-1} (A_d - I) B_c \end{aligned} \quad (36)$$

where $A_c = \frac{1}{\eta_{sd}}$ and $B_c = [\eta_{ch}, \frac{1}{\eta_{ds}}]$, and η_{sd} , η_{ch} and η_{ds} are the characteristic self-discharge constant, charge and discharge efficiencies, respectively. Since B_c defines an asymmetric behaviour in charging and discharging (even with equal charging/discharging coefficients), solving the battery scheduling requires to use two different variables for the charging and discharging powers, p_{ch} and p_{ds} , which compare in equation (26) as $\tilde{u} = [p_{ch}, p_{ds}]$. Equation (27) and (28) represent relaxed box constraints for the battery state x . The parameters $x_{min}, x_{max} \in \mathbb{R}$ are the nominal minimum and maximum capacity of the battery. The first one states that the battery's state must lie inside x_{min} and x_{max} . However, the violation of the lower bound is turned to a soft constraint thanks to the slack variable δ_e (minimized in the objective function), allowing the battery to occasionally go below the minimum state of charge. This is done to prevent the infeasibility of the problem in those cases in which the initial energy in the battery is below the minimum, as a consequence of a prolonged

unplug period and due to the self-discharging. The second constraint encodes the energy lower bound required at unplug events. Also in this case, the presence of the slack variable δ_e turns this into a soft constraint. The variable $e_{min} \in \mathbb{R}^T$ represents the minimum energy that EV is required to store, and depends on the unplugging events; in particular, the EV is required to be fully charged at unplug events, so that e_{min} can be described as:

$$e_{min,t} = \begin{cases} x_{max} & \text{if } \Delta_t x_{plug} = -1 \\ 0 & \text{otherwise} \end{cases} \quad (37)$$

Equation (30), (31) and (32) represent the operational constraints for the charging and discharging power. Here $a \in \mathbb{Z}^{T \times 2}$ is an auxiliary binary variable keeping track of activation state of charging and discharging operations. The first equation requires activations to be bounded by the presence of the car, represented by the parameter $x_{plug} \in \mathbb{R}^T$. This is equal to 1 if the EV is plugged or 0 otherwise. Equation (31) together with equation (32), encodes the complementarity constraint $p_{ch}p_{ds} = 0$ avoiding to express it as a nonlinear constraint, while bounding p_{ch} and t_{ds} inside their operational constraints.

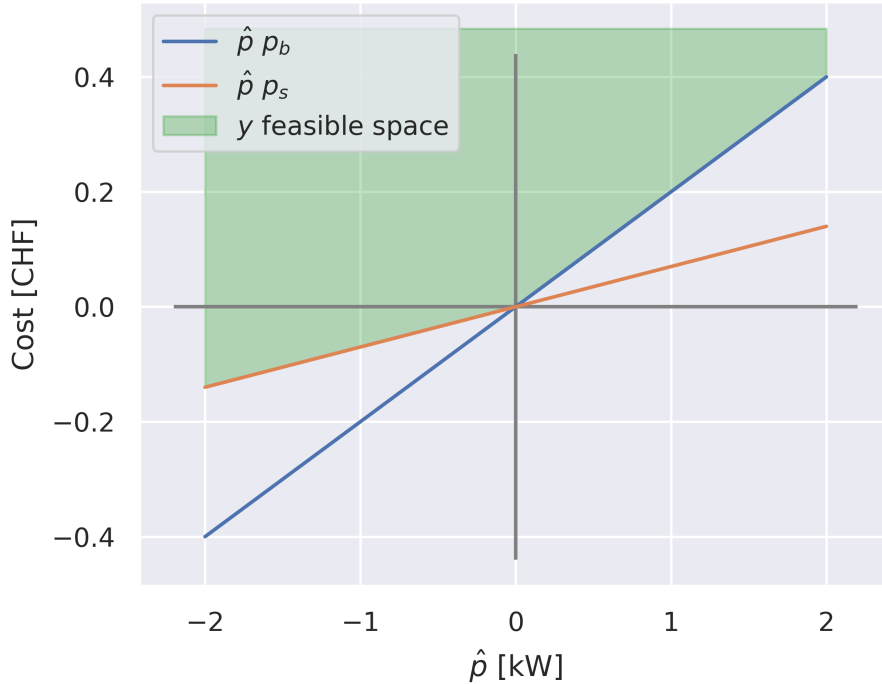


Figure 8: Visual explanation of the scope of the y variable. When linearly penalized, y is pushed to its feasible space's lower boundaries, collapsing on the cost function $c(p)$ in (41)

Finally, the last two equations (33) and (34) define the feasible space of the auxiliary

variable y . The first summation in (25) represents the total cost of the agent in the business as usual case. For prosumers, the cost function can be either positive or negative, depending on the overall power at their household's main and can be expressed as in equation (41).

$$c(p_t) = \begin{cases} p_{buy,t} p_t, & \text{if } p_t \geq 0 \\ p_{sell,t} p_t, & \text{otherwise} \end{cases} \quad (38)$$

The cost can be thought of as the maximum over two affine functions (the first and second line of equation (41), respectively). Equations (33),(34) constraint y to live in the epigraph of the maximum of these two affine functions. Minimizing y then guarantees that its value at the optimum, y^* , will lie on the epigraph's lower boundary (and will thus represents the prosumer's total costs), as shown in figure 8.

All the variables, parameters and constants of the control problem, together with their dimensionalities, are reported in table 1.

B.2 Distributed control of EVs

In this coordinated charging strategy, which applies to an energy community (EC) setting, EVs are communicating with each other and actively share their planned actions in the next control horizon to solve an optimization problem, which they jointly try to minimize. The problem can be mathematically formulated as:

$$\begin{aligned} \underset{u \in \mathcal{U}}{\operatorname{argmin}} \quad & e(u) + \sum_{i=1}^N c(u_i) \\ \text{s.t.} \quad & A_\lambda u \leq b \end{aligned} \quad (39)$$

where $\mathcal{U} = \prod_{i=1}^N \mathcal{U}_i$ is the Cartesian product of the flexible users feasible sets, $e(u)$ is a system level objective which defines the business model, $c(u_i)$ are the costs of each flexible user in the business as usual case, and $u = [u_1^T, \dots, u_N^T] = [u_i]_{i=1}^N$ is the vector of the concatenated actions of all the flexible users. Here $u \in \mathcal{U}$ means that each EVs' operations must respect the set of constraints (26)-(34). The inequality constraint in problem (39) represents system-level constraints, which can be used to encode both power and voltage grid constraints using voltage sensitivity coefficients [25].

We minimize the surplus function $e(u)$, which is the negative of the surplus that the agent community has in paying the energy at the point of common coupling with the electrical grid instead of each one paying its own separate bill:

$$e(x) = c \left(\sum_{i=1}^N u_i \right) - \sum_{i=1}^N c(u_i) \quad (40)$$

where $u_i \in \mathbb{R}^T$ is the vector of total power of the i th agent, $c(\cdot)$ is the energy cost

Name	Type	Dim.	Description
\mathbf{x}	variable	\mathbb{R}^{T+1}	battery state [kWh]
\mathbf{u}	variable	$\mathbb{R}^{T \times 2}$	charging and discharging power [kW]
\mathbf{y}	variable	\mathbb{R}^T	energy costs [£]
δ_x	variable	\mathbb{R}^T	slack variable [kWh]
δ_e	variable	\mathbb{R}^T	slack variable [kWh]
\mathbf{a}	variable	$\mathbb{Z}^{T \times 2}$	charge/discharge activation
p_{buy}, p_{sell}	parameter	\mathbb{R}^T	buying and selling prices [£/kWh]
e_{min}	parameter	\mathbb{R}^T	minimum energy due to unplug event [kWh]
\hat{p}	parameter	\mathbb{R}^T	power of uncontrolled devices [kW]
x_{start}	parameter	\mathbb{R}	initial battery state [kWh]
x_{plug}	parameter	\mathbb{R}	plug state
x_{min}, x_{max}	parameter	\mathbb{R}	capacity limits [kWh]
$\tilde{u}_{min}, \tilde{u}_{max}$	parameter	\mathbb{R}^2	charging and discharging power limits [kW]
k_1, k_2	constants	\mathbb{R}	values: 10, 1e6

Table 1: Variables, parameters and constants of the core EV optimization problem.

function defined as:

$$c(p_t) = \begin{cases} p_{b,t} p_t, & \text{if } p_t \geq 0 \\ p_{s,t} p_t, & \text{otherwise} \end{cases} \quad (41)$$

where $p_{b,t}$ and $p_{s,t}$ are the buying and selling tariffs, respectively, at time t . Prices can therefore be dynamic, given that the inequality $p_{b,t} \geq p_{s,t}$ is always respected at any point in time. Minimizing $e(u)$ maximizes the self consumption of the EC. The overall objective function for the end users (not including system-level constraints) becomes:

$$\begin{aligned} c_{tot}(u_i, u_{-i}) &= c_i(u_i) + \alpha_i e(u) \\ &= \alpha_i c \left(\sum_{i=1}^N u_i \right) + (1 - \alpha_i) c(u_i) \end{aligned} \quad (42)$$

where α is a repartition coefficient for prosumer i , which ideally defines how much of the surplus goes to the specific agent i , $\lambda_i \in \mathbb{R}^{2T}$ is a vector of Lagrangian multipliers associated with the inequality constraint in (39) and with the i_{th} agent.

Decomposing (39) using different repartition weights for the surplus, induces a game with unique generalized variational equilibrium [26], which can be reached using the preconditioned forward backward (pfb) formulation [27]. At each communication round k , agents can share their plans in order to jointly minimize their objective functions. The original pFB method can be written as reported in algorithm 1. Here $\mathcal{F}(x^k)$ is the gradient of the overall objective function for the end user (42). The Π_Z

Algorithm 1 Preconditioned forward-backward (pFB)

$$\begin{aligned} u^{k+1} &= \Pi_{\mathcal{U}_i} [u^k - \alpha(\mathcal{F}(u^k) + A^T \lambda^k)] \\ \lambda^{k+1} &= \Pi_{\mathbb{R}^+} [\lambda^k + \beta(2A_\lambda u^{k+1} - A_\lambda u^k - b)] \end{aligned}$$

in 1 stands for the projection onto the convex set Z . Since projecting on the EVs' set

of constraints (26)-(34), \mathcal{U}_i , is hard (it includes binary constraints), we reformulated the gradient descent step (the first line of algorithm (1)) as the minimization of the linearization of the system level cost around the previous state, plus a quadratic punishment on the action at the previous iteration; more details on this equivalence can be found in [14]. Replacing the agent cost with the auxiliary variable y as in (25), the final objective function (for the EV) then becomes:

$$\begin{aligned} \Phi(u_i, u^{k-1}, \lambda_i^k) = & \alpha_i \nabla c \left(\sum_{i=1}^N u_i^{k-1} \right)^T u_i + (1 - \alpha_i) \sum_{i=1}^T y_i + \lambda_i^T u_i \\ & + \rho_d \|u_i - u_i^{k-1}\|^2 + k_1 \|\delta_x\|_2^2 + k_2 \|\delta_e\|_1 \end{aligned} \quad (43)$$

where u_i^{k-1} are the agent's actions at the previous iteration. The final EVs' optimization problem can then be written as:

$$u_i^{k+1} = \underset{u_i \in \mathcal{U}_i}{\operatorname{argmin}} \Phi(u_i, u^{k-1}, \lambda_i^k) \quad (44)$$

The repartition coefficients α_i can be set in different ways. The simplest one is to them to $1/N$ where N is the number of controlled EVs. This way each agent will receive $1/n_{th}$ of the surplus. Another possibility is assign a value for α_i which depends on each agent's contribution to the surplus in the past. When all the repartition coefficients α_i in (43) are set to 1 for all the agents, this corresponds to the case in which the EVs are controlled by a central authority with the purpose of minimize the EC's costs at the point of common coupling (pcc) of the EC with the main grid, without taking into account the single individuals' costs.

B.3 Power constraints enforcement at the transformer

Explicit enforcement via lagrangian multipliers In this variant, we set up a constraint on the aggregated power of the EC. That is, A_λ in (39) was set to:

$$A_\lambda = \mathbb{I}_T \otimes \mathbb{1}_N \quad (45)$$

where \mathbb{I}_T is the identity matrix of size T , \otimes is the Kroneker product and $\mathbb{1}_N$ is the unit vector of length N , where N is the number of controlled EVs. That is, A_λ performs the summation, time-wise, of the aggregated power of all the agents. The power limit on the overall power profile was set such that EVs could respect it most of the times; this was computed using information about the total capacity of the EVs and historical data of the uncontrolled power profile.

Power tariff at the PCC An possibility to enforce peak shaving and valley filling at the coupling point is to apply a power based tariff at the coupling point. This would

add a quadratic term the cost equation (41) at the PCC, which will become:

$$c(p_t) = \begin{cases} (p_{buy,t} + \gamma p_t) p_t, & \text{if } p_t \geq 0 \\ (p_{sell,t} + \gamma p_t) p_t, & \text{otherwise} \end{cases} \quad (46)$$

where γ is a quadratic punishment coefficient. To enforce this pricing scheme, we need to add a quadratic punishment on the overall power profile to the system level objective. This can directly be included in the pFB algorithm, adding the following term in equation (43):

$$\alpha_i \gamma \left(\sum_{i=1}^N u_{i,k-1} \right)^T \quad (47)$$

References

- [1] A. Navarro and H. Rudnick, "Large-Scale Distribution Planning Part I: Simultaneous Network and Transformer Optimization," *IEEE Transactions on Power Systems*, vol. 24, no. 2, pp. 744–751, 2009.
- [2] A. Seack, J. Kays, and C. Rehtanz, "Generating Low Voltage Grids on the Basis of Public Available Map Data," *Proceedings of the CIRED Workshop 2014: Challenges of Implementing Active Distribution System Management*, no. June, pp. 11–12, 2014.
- [3] C. Mateo Domingo, T. Gómez San Román, Á. Sánchez-Miralles, J. P. Peco González, and A. Candela Martínez, "A reference network model for large-scale distribution planning with automatic street map generation," *IEEE Transactions on Power Systems*, vol. 26, no. 1, pp. 190–197, 2011.
- [4] M. Yu, A. Hillebrand, P. Tewarie, J. Meier, B. van Dijk, P. Van Mieghem, and C. J. Stam, "Hierarchical clustering in minimum spanning trees," *Chaos*, vol. 25, no. 2, pp. 1–10, 2015.
- [5] J. A. Lukes, "Efficient Algorithm for the Partitioning of Trees," *IBM Journal of Research and Development*, vol. 18, no. 3, pp. 217–224, may 1974.
- [6] "Merkblatt SIA 2024: Raumnutzungsdaten für die Energie- und Gebäudetechnik," SIA Schweizerischer Ingenieur- und Architektenverein, standard, 2015.
- [7] T. Afjei, U. Schonhardt, C. Wemhöner, M. Erb, H. R. Gabathuler, H. Mayer, G. Zweifel, M. Achermann, R. von Euw, and U. Stöckli, "Standardschaltungen für Kleinwärmepumpenanlagen Teil 2: Grundlagen und Computersimulationen. Schlussbericht," Tech. Rep., 2002.
- [8] L. Girardin, "A GIS-based Methodology for the Evaluation of Integrated Energy Systems in Urban Area," p. 218, 2012. [Online]. Available: <http://infoscience.epfl.ch/record/170535>
- [9] K. Arendt, M. Jradi, H. R. Shaker, C. T. Veje, and S. Denmark, "Comparative Analysis of white-, gray- and black-BOX models for thermal simulation of indoor environment: teaching building case study," in *Building Performance Modeling Conference*, 2018, pp. 173–180.
- [10] G. Reynders, J. Diriken, and D. Saelens, "Quality of grey-box models and identified parameters as function of the accuracy of input and observation signals," *Energy and Buildings*, vol. 82, pp. 263–274, 2014. [Online]. Available: <http://dx.doi.org/10.1016/j.enbuild.2014.07.025>
- [11] P. Bacher and H. Madsen, "Identifying suitable models for the heat dynamics of buildings," *Energy and Buildings*, vol. 43, no. 7, pp. 1511–1522, 7 2011. [Online]. Available: <http://linkinghub.elsevier.com/retrieve/pii/S0378778811000491>
- [12] T. Schütz, H. Harb, R. Streblov, and D. Müller, "Comparison of models for thermal energy storage units and heat pumps in mixed integer linear programming," 2015.
- [13] J. S. Stein, "The photovoltaic Performance Modeling Collaborative (PVP/MC)," *Conference Record of the IEEE Photovoltaic Specialists Conference*, pp. 3048–3052, 2012.

- [14] L. Nespoli, M. Salani, and V. Medici, "A rational decentralized generalized Nash equilibrium seeking for energy markets," in *2018 International Conference on Smart Energy Systems and Technologies, SEST 2018 - Proceedings*, 2018.
- [15] L. Nespoli and V. Medici, "Constrained hierarchical networked optimization for energy markets," in *Proceedings - 2018 IEEE PES Innovative Smart Grid Technologies Conference Europe, ISGT-Europe 2018*, 2018.
- [16] H. Queiroz, R. A. Lopes, and J. Martins, "Automated energy storage and curtailment system to mitigate distribution transformer aging due to high renewable energy penetration," *Electric Power Systems Research*, vol. 182, p. 106199, 2020.
- [17] "sccer furies deliverable d1.2.5a-b: Chapter(s) on the design and test of distributed dsm algorithms that use communication and new forecasting models," Tech. Rep.
- [18] "EN 50160, Voltage characteristics of electricity supplied by public distribution systems," European Committee for Electrotechnical Standardization (CENELEC), standard, 1999.
- [19] F. P. Incropera, D. P. DeWitt, T. L. Bergman, and A. S. Lavine, *Fundamentals of Heat and Mass Transfer*, 2007.
- [20] T. Cholewa, M. Rosiński, Z. Spik, M. R. Dudzińska, and A. Siuta-Olcha, "On the heat transfer coefficients between heated/cooled radiant floor and room," *Energy and Buildings*, vol. 66, pp. 599–606, 2013.
- [21] P. Wallenten, "Heat Transfer Coefficients in a Full Scale Room With and Without Furniture," *Lund Institute of Technology*, pp. 1–8, 1999.
- [22] R. D. Coninck, R. Baetens, D. Saelens, A. Woyte, L. Helsens, A. Mechanics, and B. P. Section, "Rule-based demand side management of domestic hot water production with heat pumps in zero energy neighbourhoods," *Journal of Building Performance Simulation*, 2013.
- [23] L. Nespoli, A. Giusti, N. Vermes, M. Derboni, A. Rizzoli, L. Gambardella, and V. Medici, "Distributed demand side management using electric boilers," *Computer Science - Research and Development*, vol. 32, no. 1-2, 2017.
- [24] L. S. Shieh, H. Wang, and R. E. Yates, "Discrete-continuous model conversion," *Topics in Catalysis*, 1980.
- [25] K. Christakou, J. Y. Leboudec, M. Paolone, and D. C. Tomozei, "Efficient computation of sensitivity coefficients of node voltages and line currents in unbalanced radial electrical distribution networks," *IEEE Transactions on Smart Grid*, vol. 4, no. 2, pp. 741–750, 2013.
- [26] L. Nespoli, M. Salani, and V. Medici, "A rational decentralized generalized Nash equilibrium seeking for energy markets," in *2018 International Conference on Smart Energy Systems and Technologies, SEST 2018 - Proceedings*. Institute of Electrical and Electronics Engineers Inc., 10 2018.
- [27] G. Belgioioso and S. Grammatico, "Projected-gradient algorithms for Generalized Equilibrium seeking in Aggregative Games are preconditioned Forward-Backward methods," *arXiv*, 2018.